

Topologically protected Bell-cat states in a simple spin model

B. Lajci,¹ D. H. J. O'Dell,¹ and J. Mumford^{1,2,3}

¹*Department of Physics and Astronomy, McMaster University,
1280 Main St. W., Hamilton, ON, L8S 4M1, Canada*

²*Homer L. Dodge Department of Physics and Astronomy,
The University of Oklahoma, Norman, Oklahoma 73019, USA*

³*Center for Quantum Research and Technology, The University of Oklahoma, Norman, Oklahoma 73019, USA*

(Dated: November 1, 2024)

We consider the topological properties of the so-called central spin model that consists of N identical spins coupled to a single distinguishable central spin which arises in physical systems such as circuit-QED and bosonic Josephson junctions coupled to an impurity atom. The model closely corresponds to the Su-Schrieffer-Heeger (SSH) model except that the chain of sites in the SSH model is replaced by a chain of states in Fock space specifying the magnetization. We find that the model accommodates topologically protected eigenstates that are ‘Bell-cat’ states consisting of a Schrödinger cat state of the N spins that is maximally entangled with the central spin, and show how this state can be adiabatically created and moved along the chain by driving the central spin. We visualize the Bell-cat states by plotting their Wigner function and also show their robustness against random noise by solving the master equation for the density matrix.

I. INTRODUCTION

A cat state is a coherent superposition of two or more quantum states that exhibit significant differences on a macroscopic scale. Initially introduced in a thought experiment by Erwin Schrödinger [1] to underscore the striking distinctions between quantum and classical physics, cat states became a useful concept in philosophical discussions about the interpretations of quantum mechanics. More recently, progress in controlling quantum systems at the level of single atoms and photons has led to the successful realization of cat states in experiments. These include the superposition of a single laser cooled ion in two spatially separated locations [2], and the superposition of two or more coherent states of photons localized in different regions of phase space in a light pulse [3], in microwave fields in cavities [4], and in circuit-QED systems [5]. Additionally, cat states have been created using the spin degrees of freedom of trapped ions [6], and also by placing the vibrational state of a trapped ion in a coherent superposition dependent on its internal spin [8–10]. Such entanglement between different types of degrees of freedom has also been achieved between the polarization of spatial mode degrees of freedom with photons [11].

This progress in our ability to generate and control quantum states has technological implications because cat states formed from a pair of coherent states have the potential to be used as qubits [12]. When sufficiently separated, each coherent state has exponentially small overlap, so they can form the basis states $|0\rangle$ and $|1\rangle$ of the qubit. Coherent states have significantly larger Hilbert spaces than traditional qubits which allows for the possibility of encoding other information within these superpositions, and in some cases, facilitating more effective error correction protocols.

A widely implemented technique for creating cat states involves the use of an ancillary qubit. The first step is

to initialize the qubit in an equal superposition of its two states, which for an atomic qubit would be achieved by applying a $\pi/2$ laser pulse, and the second step is to entangle the qubit with a coherent state of a larger quantum system, thereby generating a cat state in the latter system. This can be accomplished by making the phase of the coherent state dependent on the state of the qubit. For example, a force applied to a mechanical oscillator that depends on the state of a qubit can generate a macroscopic superposition of two coherent states of phonons where each coherent state has a different phase [13], or the state of an atom resonantly coupled to an optical cavity can be used to apply a phase flip to incoming coherent pulses of light [14]. In numerous instances, the interaction between the ancillary qubit and the coherent state results in maximal entanglement between the two, giving rise to states known as Bell-cat (BC) states, see [15] and references therein (these states are also known by other names such as squeezed wavepacket entangled states [9]). BC states represent more complex counterparts to regular Bell states, which in their original setting are maximally entangled states only of pairs of qubits. The complexity arises from the fact that coherent states possess more degrees of freedom than a single qubit, and this has led to BC states being employed in research exploring information extraction and entanglement generation beyond the scope of qubit Bell states [15]. The continuous nature of the relative phase between coherent states means BC states might find a role in the continuous variable form of quantum information processing [16].

In this paper, we show that a BC state can be created via adiabatic driving in a simple version of the Mermin central spin (CS) model [17–20]. The CS model consists of a central two-state particle playing the role of the ancillary qubit surrounded by N identical non-self-interacting two-state particles. The driving protocol makes use of two important features of the system: (1) There is a

topological phase transition where the topologically non-trivial phase hosts a pair of zero energy bound states in the Fock space of the identical spins; (2) The inhomogeneity of the Fock space of the identical spins allows one to vary the locations of the bound states by tuning the strength of an the applied magnetic field.

Highly controllable versions of the CS model can potentially be realized experimentally using the physical systems already mentioned. For example, the two polarization states of photons means they can naturally play the role of the non-self-interacting two-state particles. Alternatively, the two topologically distinguished clockwise and anticlockwise orbital angular momentum states of photons in a structured Gaussian light beam can also act in this capacity [21, 22]. Coupling photons to a real atom [4], or a circuit-QED setup in the form of a superconducting transmon qubit in a microwave waveguide cavity resonator [5, 15], would allow the realization of the CS model, as would the spin-motion entanglement that can be utilized in trapped ion systems [9].

Yet another way to realize the CS model is using ultracold atoms, for example by immersing an atomic quantum dot in a two-state Bose-Einstein condensate (BEC), the latter also being known as a bosonic Josephson junction. The two states of the BEC atoms can either be two internal spin states [23] or two external modes (double well potential) [24, 25], and the atomic quantum dot can be a single impurity atom [26–31] or ion [32–34] that also has either two internal or two external states. Feshbach resonances can be used to independently control the boson-boson interactions and impurity-boson interactions. Recent experimental realizations of the controlled coupling between individual localized Cs impurity atoms immersed in a Rb BEC in have been reported in references [35–37]. We also note that bosonic Josephson junctions can also be realized using structured light in an aberrated optical cavity [38].

II. MODEL

The system we will be investigating is a version of the CS model which describes N identical two-state particles interacting with a distinguishable central two-state particle. Due to each particle having access to two states, we will refer to them as spin-1/2 particles. The N identical spins do not interact with each other, but interact equally with the CS leading to the Hamiltonian

$$\hat{H} = v\hat{\sigma}_x + \frac{2w}{N} \left(\hat{S}_+\hat{\sigma}_- + \hat{S}_-\hat{\sigma}_+ \right) \quad (1)$$

where the CS operators are represented explicitly as Pauli matrices and the large spin is represented as the sum of the identical spins' Pauli matrices $\hat{S}_\pm = \sum_i^N \hat{\sigma}_\pm^i$. The parameters v and w represent the CS spin-flip energy and the energy of the spin-exchange between the CS and identical spins, respectively. We will work in the eigenbasis of

the \hat{S}_z and $\hat{\sigma}_z$ operators, $\{|n, m\rangle\}$, where $n = (N_\uparrow - N_\downarrow)/2$ is half the difference between the number of up and down identical spins and $m = \uparrow, \downarrow$ are the two states of the CS. This basis defines the Fock states of the system and physically speaking it gives the magnetization along the z axis.

The usefulness of this basis comes from the fact that the CS model bears a close resemblance to the Su-Schrieffer-Heeger (SSH) model [7] which describes the electronic properties of a 1D polymer with alternating single and double bonds. Under this comparison the Fock state label n is analogous to the unit cell label and m is analogous to the intra-unit cell label. In addition, like the SSH model, the CS model undergoes a topological phase transition from a trivial phase when $v > w$ to a nontrivial phase when $v < w$ which is marked by the presence of a pair of topologically protected bound states with energy $E = 0$. However, unlike the SSH model whose bound states only appear at the edges of the polymer, the CS model's bound states can be centered at any value of n . Their protection relies on the chiral symmetry which the Hamiltonian in Eq. (1) obeys and is defined in terms of the chiral operator $\hat{\sigma}_z$ and the relation $\hat{\sigma}_z \hat{H} \hat{\sigma}_z = -\hat{H}$. The chiral symmetry means that $\hat{\sigma}_z$ transforms states with energy E to states with energy $-E$ and since the bound states have $E = 0$, they are eigenstates of $\hat{\sigma}_z$. This also means that each bound state exists entirely in either the CS \uparrow or \downarrow subspace and that any perturbations respecting the chiral symmetry will not destroy them.

In condensed matter systems, topologically protected bound states are well localized in the material. For now we will assume that the same is true for the protected bound states in the Fock space of the CS model and provide evidence for it later. The assumption of localization allows us to take a mean field approximation of the identical spins' operators by taking their coherent spin expectation values

$$\langle \theta, \phi | \hat{\mathbf{S}} | \theta, \phi \rangle = \frac{N}{2} (\sin \theta \cos \phi, \sin \theta \sin \phi, \cos \theta). \quad (2)$$

This approximation labels the states of the identical spins as points on the surface of a spin- $N/2$ Bloch sphere where θ and ϕ are the polar and azimuthal angles, respectively. The mean field approximation of Eq. (1) is

$$\mathcal{H}(\theta, \phi) = \mathbf{d}(\theta, \phi) \cdot \hat{\boldsymbol{\sigma}} \quad (3)$$

where $\hat{\boldsymbol{\sigma}} = (\hat{\sigma}_x, \hat{\sigma}_y, \hat{\sigma}_z)$ and the vector $\mathbf{d}(\theta, \phi) = (d_x(\theta, \phi), d_y(\theta, \phi), d_z(\theta, \phi))$ has components

$$\begin{aligned} d_x(\theta, \phi) &= v + w \sin \theta \cos \phi, & d_y(\theta, \phi) &= w \sin \theta \sin \phi, \\ d_z(\theta, \phi) &= 0. \end{aligned} \quad (4)$$

Equation (3) resembles a Bloch Hamiltonian of a two-band model describing a periodic lattice under the tight-binding approximation, however, there is one major difference. In a typical Bloch Hamiltonian the vector \mathbf{d}

is parameterized by the quasi-momentum which is 2π -periodic, so it maps points from a circle (1D) or a torus (2D) to, in general, a 3D vector, whereas \mathbf{d} in Eq. (3) maps points from the mean-field Bloch sphere to a 2D vector (because $d_z = 0$). The azimuthal angle ϕ is indeed 2π -periodic, so it plays the role of a quasi-momentum in the CS model, but the polar angle θ is not 2π -periodic, so it cannot be considered as another quasi-momentum. Instead, it gives the ‘position’ in Fock space from the relation $n = \frac{N}{2} \cos \theta$.

In 1D lattice models which undergo a topological phase transition, the transition is quantified in terms of the winding number which answers the question, how many times does \mathbf{d} wind around its origin as the quasi-momentum is cycled through its range once. Due to the fact that \mathbf{d} maps one periodic surface to another, the winding number takes integer values and is nonzero in the topologically nontrivial phase. In the SSH model, the components of \mathbf{d} can be written in a similar form to Eq. (4), but with θ fixed to $\theta = \pi/2$ and $\phi \rightarrow k$ where k is the quasimomentum of the lattice:

$$\begin{aligned} d_x^{\text{SSH}}(k) &= v + w \cos k, & d_y^{\text{SSH}}(k) &= w \sin k, \\ d_z^{\text{SSH}}(k) &= 0. \end{aligned} \quad (5)$$

Therefore, as k varies by 2π , \mathbf{d} traces out a circle of radius w in the d_x, d_y plane centered at $(v, 0)$. When $v < w$, the circle encloses the origin and the winding number is unity which signifies that the system is in the topologically nontrivial phase. The components of \mathbf{d} for the CS model are more general than those of the SSH model, however, we can ask a similar question: how many times does \mathbf{d} wind around the origin of the d_x, d_y plane for *any* fixed value of θ as ϕ varies by 2π . We answer this question with an explicit calculation of the winding number

$$\begin{aligned} W(\theta) &= \frac{1}{2\pi} \int_0^{2\pi} \left(\hat{\mathbf{d}}(\theta, \phi) \times \frac{d}{d\phi} \hat{\mathbf{d}}(\theta, \phi) \right)_z d\phi \\ &= \frac{1}{2} [1 + \text{sgn}(w \sin \theta - v)] \end{aligned} \quad (6)$$

where $\hat{\mathbf{d}} = \mathbf{d}/|\mathbf{d}|$. The topologically trivial phase is marked by $W = 0$ which occurs when $v > w$ and the topologically nontrivial phase is marked by $W = 1$ which occurs when $v < w$. However, due to the θ dependence of the winding number, only part of the Bloch sphere of the identical spins has nontrivial topology in the latter case. The nontrivial part lies in the range $\theta_1 < \theta < \theta_2$ where $\theta_1 = \arcsin(v/w)$ and $\theta_2 = \pi - \arcsin(v/w)$ and outside of this range there is trivial topology. The boundary angles mark the polar coordinates on the Bloch sphere of topologically protected bound states [7] and we emphasize that the appearance of a single bound state at each boundary provides support for the bulk-boundary correspondence. The correspondence asserts that a bulk topological invariant, such as the winding number, determines the number of bound states at a particular boundary separating two regions of different topology. In the

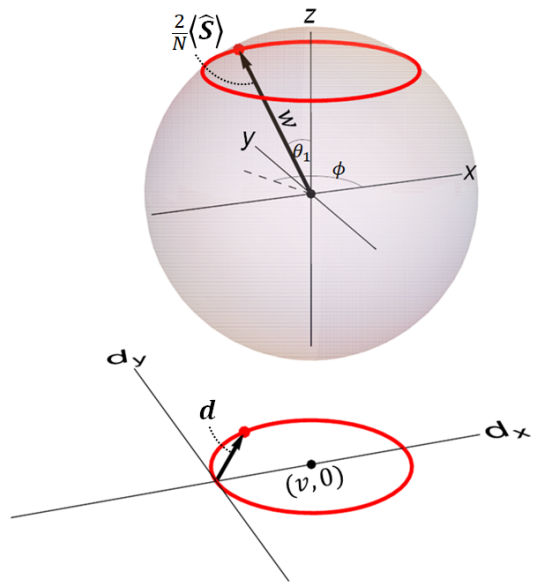


FIG. 1. Geometric representation of the mean-field Hamiltonian. The vector pointing from the origin of the sphere to its surface represents the mean field state of the identical spins while the direction of the vector \mathbf{d} in the d_x, d_y plane gives the eigenstate of the mean-field Hamiltonian. For a fixed value of θ , as ϕ changes by 2π , the sphere vector traces out a circuit (red). The vector \mathbf{d} follows the same path, but projected directly down onto the d_x, d_y plane. When the projected circuit encompasses the origin of the plane, the system is in the topologically nontrivial phase with winding number $W = 1$. The red circle at $\theta = \theta_1$ is the boundary circuit between the topologically trivial and nontrivial phases where any circle with a larger radius will encompass the origin.

CS model, the presence of two boundaries is a consequence of the existence of two ‘edges’ in the Fock space of identical spins located at $n_{\text{edge}} = \pm N/2$.

Figure 1 gives a geometric interpretation of the topological properties of the system. The vector extending from the sphere’s center to its surface is $\frac{2}{N} \langle \hat{S} \rangle$ (scaled by w) and represents the mean field state of the identical spins while the vector in the d_x, d_y plane is $\mathbf{d}(\theta, \phi)$ whose direction denotes the eigenstate of the mean-field Hamiltonian in Eq. (3). For a fixed value of θ , as ϕ changes by 2π , the vector on the sphere traces out a circle on its surface and the vector $\mathbf{d}(\theta, \phi)$ traces the same path projected directly down onto the d_x, d_y plane. The d_x coordinate of the center of the sphere is v , whereas the sphere’s radius is w . When $v > w$, the projected path fails to enclose the origin of the plane, causing $\mathbf{d}(\theta, \phi)$ to oscillate without fully winding as ϕ changes by 2π . When $v < w$, there exist certain values of θ for which the trajectory projected onto the plane encircles the origin, causing $\mathbf{d}(\theta, \phi)$ to wrap around the origin once. The range of θ exhibiting nonzero winding is $\theta_1 < \theta < \theta_2$, with the boundaries determined by the points where the projected trajectory intersects the origin of the plane. In Figure 1, the red circles represent the trajectories for

$\theta = \theta_1$ and show that when $\phi = \pi$, $|\mathbf{d}(\theta_1, \pi)| = 0$ leading to the intersection of the trajectory with the origin and the closure of the energy gap, $E_{\text{gap}} = 2|\mathbf{d}|$, at that point. Although not shown, due to the spherical symmetry, the same thing happens at $(\theta, \phi) = (\theta_2, \pi)$. Consequently, these points correspond to the locations of the protected bound states.

Figure 1 also gives a clear picture of how modifications to Eq. (1) affect the topological properties of the system. For instance, if the term $u\hat{\sigma}_y$ is introduced, then the center of the sphere will have its coordinates shifted to (v, u) in the plane. The condition for the existence of a non-trivial topological region is that the radius of the sphere be larger than the distance from the origin to its center projected onto the d_x, d_y plane which means the topological phase transition will occur at $w = \sqrt{v^2 + u^2}$. Having nonzero u also changes the direction from the origin to the sphere, so the gap will no longer close at $\phi = \pi$, but at the more general angle $\phi = \pi + \arctan(u/v)$. Note that such a change preserves the chiral symmetry of the Hamiltonian and in turn preserves the existence of protected bound states. Modifications that introduce terms proportional to $\hat{\sigma}_z$ break the chiral symmetry by lifting the projected trajectories out of the d_x, d_y plane, so they are no longer forced to intersect the origin. In that case, the energy gap no longer closes and the protected bound states no longer exist.

III. RESULTS

A. Bound state fluctuations

Before moving on to describing our protocol for the the creation of BC states we will confirm the existence of the protected bound states discussed in the previous section. The mean field analysis determined the locations of the bound states, however, we would also like to know about their fluctuations to determine how localized they are. For that, we use the fact that the bound states are zero energy eigenstates and exist entirely in one of the CS subspaces, so $\mathcal{H}(n, \phi)\chi_{\uparrow(\downarrow)}(n) = 0$ where

$$\begin{aligned} \chi_{\uparrow}(n) &= B_{\uparrow}(n) \begin{bmatrix} 1 \\ 0 \end{bmatrix} \\ \chi_{\downarrow}(n) &= B_{\downarrow}(n) \begin{bmatrix} 0 \\ 1 \end{bmatrix}. \end{aligned} \quad (7)$$

The bound states are written as products of the wave function in the identical spins' Fock space $B_{\uparrow(\downarrow)}(n)$ and a two component vector for the two states of the spin-1/2 particle. Note that we have changed from the polar coordinate, θ , to the \hat{S}_z state label, n , through the relation $n = \frac{N}{2} \cos \theta$ which will be useful in the coming calculations. In the n state space the bound states are located at $n_1 = n_b$ and $n_2 = -n_b$ where $n_b = \frac{N}{2} \sqrt{1 - (\frac{v}{w})^2}$. We are interested in fluctuations around the gap closing

point at $\phi = \pi$, so we expand $\mathcal{H}(n, \phi)$ to linear order around this point. In addition, we incorporate fluctuations into the mean-field approximation by making use of the fact that n and ϕ are conjugate variables so the transformation $\phi \rightarrow i \frac{\partial}{\partial n}$ can be made resulting in the differential equation

$$\left[\left(v - w \sqrt{1 - \left(\frac{2n}{N} \right)^2} \right) \hat{\sigma}_x - w \sqrt{1 - \left(\frac{2n}{N} \right)^2} \left(i \frac{\partial}{\partial n} - \pi \right) \hat{\sigma}_y \right] \chi_{\uparrow(\downarrow)}(n) = 0 \quad (8)$$

The wave functions $B_{\uparrow(\downarrow)}(n)$ can be solved for exactly and are of the form $B_{\uparrow}(n) \propto e^{i\pi n} e^{n - \frac{Nv}{2w} \arcsin(\frac{2n}{N})}$ where $B_{\downarrow}(n) = B_{\uparrow}(-n)$, however, they are only valid in the region around $\pm n_b$, so we expand them around those points giving

$$B_{\uparrow(\downarrow)}(n) \approx (2\pi\sigma^2)^{-1/4} e^{i\pi n} e^{-\frac{(n \pm n_b)^2}{4\sigma^2}} \quad (9)$$

where $\sigma = \sqrt{\frac{Nv^2}{4w^2 \sqrt{1 - (\frac{v}{w})^2}}}$ is the standard deviation of the wave function. The bound states take the form of Gaussians centered at the gap closing locations with widths that scale as $1/\sqrt{N}$ relative to N , so for a sufficiently large number of identical spins, they are well localized. The presence of the $[1 - (v/w)^2]^{-1/2}$ factor in σ also indicates that the bound states become increasingly localized as the system moves deeper into the topologically nontrivial phase. Indeed, in the limit $v/w \rightarrow 0$ the bound states are Fock states located at $\pm N/2$. As shown in Figure 1, in this limit, the Bloch sphere sits directly above the origin of the plane, resulting in the bound states being positioned at the North and South poles of the Bloch sphere.

Figure 2(a) shows $P_{\uparrow}(n, E) = |\langle E|n, \uparrow\rangle|^2$ which is the probability for a Fock state to have energy E in the CS \uparrow subspace. Two lobes are shown at positive and negative energies with a single bound state between them at $E = 0$. Panel (b) shows the same figure except in the CS \downarrow subspace where the only difference is that the bound state is located on the other side of $n = 0$. Panel (c) shows the $E = 0$ slice of both (a) and (b), $P(n) = |\langle E = 0|n, \uparrow\rangle + \langle E = 0|n, \downarrow\rangle|^2/2$, where the red circles and blue triangles are data from the diagonalization of Eq. (1), while the solid lines are $|B_{\uparrow}(n)|^2$ and $|B_{\downarrow}(n)|^2$ from Eq. (9), respectively. There is excellent agreement between the analytic and numerical results, and this is expected to hold as long as the system remains away from the topological phase transition point at $v = w$. This is because, as previously mentioned, the width of the bound states is predicted to diverge at this point, leading to

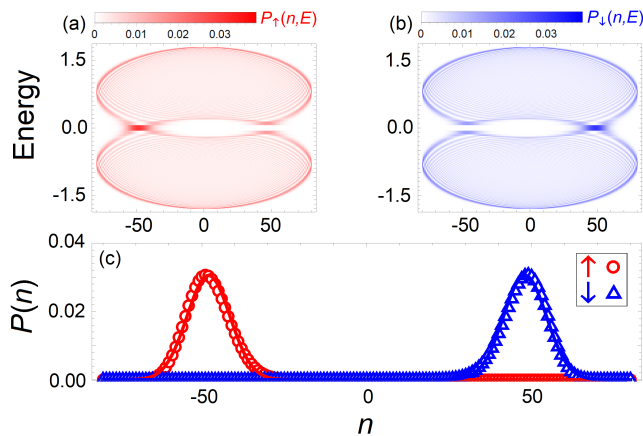


FIG. 2. Probability distributions in the Fock and energy bases. (a) Probability for a Fock state to have a given energy in the CS \uparrow subspace, $P_{\uparrow}(n, E) = |\langle E|n, \uparrow\rangle|^2$. (b) Same as (a), but in the CS \downarrow subspace, $P_{\downarrow}(n, E) = |\langle E|n, \downarrow\rangle|^2$. (c) Probability distributions of the zero energy bound states where the left and right distributions are in the CS \uparrow (red circles) and \downarrow (blue triangles) subspaces, respectively. The parameter values are $N = 180$, $w = 1$ and $v = 0.7$.

discrepancies between the analytic and numerical results due to finite size effects.

B. Generating BC states

The protocol we use to generate BC states can be broken down into three steps. (1) The system is initialized in the topologically trivial phase ($v > w$) in the product state

$$|\psi(0)\rangle = |\pi/2, \pi\rangle \otimes (|\uparrow\rangle + |\downarrow\rangle) / \sqrt{2} \quad (10)$$

where $|\pi/2, \pi\rangle$ is the spin coherent state centered at $(\theta, \phi) = (\pi/2, \pi)$ on the Bloch sphere. For large N , the coherent part has a Gaussian shape centered at $n = 0$ in the \hat{S}_z basis

$$\langle n|\pi/2, \pi\rangle \approx (\pi N/2)^{-1/4} e^{i\pi n} e^{-\frac{n^2}{N}}. \quad (11)$$

Our motivation for starting the process in the trivial phase comes from the fact that eigenstates of the Hamiltonian which will become the topologically protected bound states are centered at $\theta = \pi/2$ ($n = 0$ in Fock space) and $\phi = \pi$ on the Bloch sphere in the trivial phase. Furthermore, we start with an equal superposition of the two CS states because we recall that in the nontrivial phase each of the two bound states is in opposite subspaces of the CS. (2) Next, we adiabatically drive the system into the topologically nontrivial phase by linearly driving the CS spin-flip energy, $v(t) = v_0 - \gamma t$, where v_0 is the initial value of v and γ is the drive rate. Because the initial state is in a superposition of the CS being both

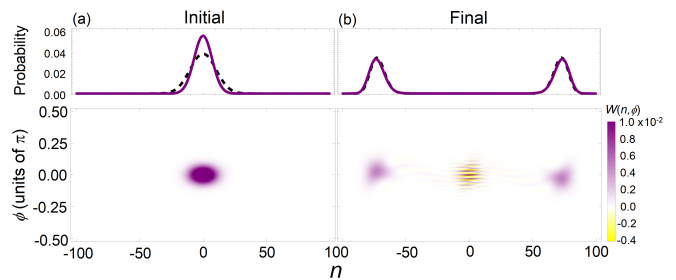


FIG. 3. Wigner quasi-probability distributions. (a) The bottom panel shows the sum of the naught and x components of the joint Wigner quasi-probability distribution of the spin coherent state $|\pi/2, \pi\rangle$. The top panel shows the probability distribution of the coherent state in Fock space (solid purple) and the even parity bound state (dashed black) in the topologically trivial phase where $v = 1.3$. (b) The top and bottom panels show the same as (a), but for the final state at the end of the driving period. The parameters are $\gamma \approx 1.2 \times 10^{-3}$, $v_0 = 1.3$ and $v_f = 0.7$. The dashed black curve in the top panel is the even parity bound state in the topologically nontrivial phase where $v = 0.7$. In all panels $w = 1$ and $N = 200$.

up and down, the wave function will split in two with each part being attached to $B_{\uparrow}(n)$ and $B_{\downarrow}(n)$. (3) After some time when the two parts of the wave function have negligible overlap, they are in a macroscopic superposition of the majority of the identical spins pointing up and pointing down. The splitting process relies on the fact that the topological bound states are protected by the chiral symmetry and are therefore eigenstates of $\hat{\sigma}_z$. This forces the bound states on opposite sides of $n = 0$ to have support in opposite CS subspaces resulting in the formation of a BC state.

To illustrate the initial and final steps of the splitting process we calculate the joint Wigner quasi-probability distribution

$$W_i(n, \phi_p) = \frac{1}{N+1} \sum_{n'} \langle n - n' | \rho_i | n + n' \rangle e^{2i\phi_p n'}. \quad (12)$$

which gives the state of the system in the space of conjugate variables (n, ϕ) and is similar to the phase space of classical systems. The phase $\phi_p = \frac{2\pi p}{N+1}$ is the discrete version of the azimuthal angle of the identical spins' Bloch sphere and $\rho_i = \text{Tr}_{\text{CS}} [\hat{\sigma}_i \rho]$ where $i = 0, x, y, z$. In experiments, a complete representation of a given state requires all four distributions. However, for visualizing both the distribution splitting and quantum correlations, only $W_0(n, \phi_p)$ and $W_x(n, \phi_p)$ are necessary. Both are combined in Figure 3, where the lower part of (a) illustrates the initial state with $\rho(0) = |\psi(0)\rangle\langle\psi(0)|$, and the lower part of (b) depicts the final state once the driving has stopped.

The central region of the lower part in (b) displays negative values originating from $W_x(n, \phi_p)$, a distinctive feature reflecting quantum correlations in the Wigner distribution. The two blobs on opposite sides of $n = 0$ rep-

represent the macroscopic superposition. Together, these distributions clearly indicate the formation of a cat state. The solid purple curve in the top of both (a) and (b) show $\sum_p W_0(n, \phi_p)$ which is the probability distribution in the identical spins' Fock space. The dashed black curves are the probability distributions of the bound states, representing the target states. There is excellent overlap between the evolved and target distributions following the driving in (b).

Two primary factors influencing the quality of the final BC state are adiabaticity and the overlap between the initial coherent state and the eigenstates which will become the bound states. In Figure 4 (a), the energy spectrum as a function of v is shown, with the red and black curves representing the energies of the bound and bulk states, respectively. Adiabaticity can be maintained as long as the driving rate is considerably smaller than the minimum gap. While the gap does close between the two $E = 0$ eigenstates, they are even and odd superpositions of the two bound states, so they possess opposite parity. As the initial coherent state has even parity under the transformation $n \rightarrow -n$ and flipping of the CS, it has significant overlap with only the even superposition over the course of the dynamics. With adiabaticity satisfied, the fidelity of the final state is determined by the fidelity of the initial state. In the topologically trivial phase, the identical spins' component of the eventual bound states takes the form of Eq. (9) with $n_b = 0$ and $\sigma = \sqrt{\frac{N}{4\sqrt{1-\frac{w}{v}}}}$ (see Appendix A for calculation), so when $v \gg w$, the standard deviation is $\sigma \approx \sqrt{N/4}$ and they are approximately equal to the initial coherent state in Eq. (11). Thus, the quality of the final BC state improves as the system is initialized deeper within the topologically trivial phase, which corresponds to larger initial values of v . This trend is illustrated in Figure 4 (b), where the final fidelity is displayed to asymptotically approach unity as $v_0 \rightarrow \infty$.

C. Replacing the identical spins with a single bosonic mode

Coherent cat states of light have been achieved using a variety of methods, so it is important to determine whether it is possible to do the same using our protocol. To this end, we replace the identical spin operators in Eq. (1) with operators of a single bosonic mode, $2\hat{S}_-/N \rightarrow \hat{a}$ and $2\hat{S}_+/N \rightarrow \hat{a}^\dagger$, where \hat{a}^\dagger (\hat{a}) is the creation (annihilation) operator of the mode obeying the usual commutation relation $[\hat{a}, \hat{a}^\dagger] = 1$. The Hamiltonian becomes

$$\hat{H} \rightarrow \hat{H}_a = v\hat{\sigma}_x + w(\hat{a}^\dagger\hat{\sigma}_- + \hat{a}\hat{\sigma}_+). \quad (13)$$

where the term proportional to w is now in the form of a Jaynes-Cummings interaction which is found in the system of a qubit interacting with a single mode of an optical cavity and describes the absorption and stimulated

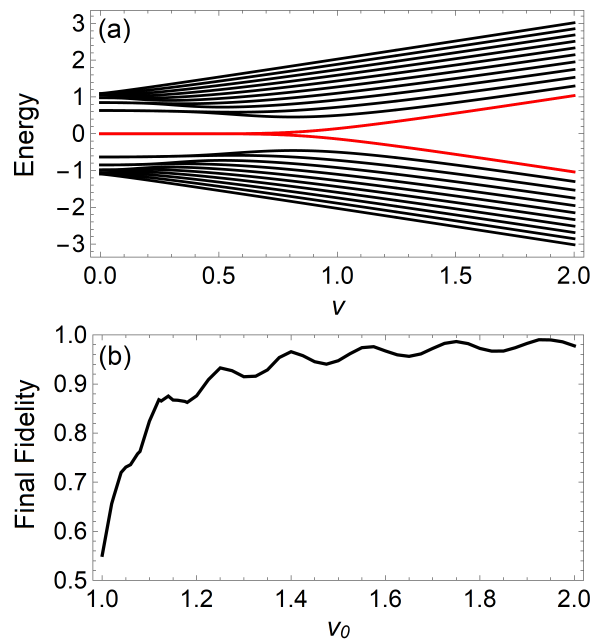


FIG. 4. Energy spectrum and final state fidelity. (a) Energy spectrum as a function of the CS spin-flip energy v . The red and black curves represent the energies of the bound and bulk states, respectively. The parameters are $N = 10$ and $w = 1$. (b) Fidelity between the final state at the end of the driving period and the instantaneous bound state with even parity. The parameters are $N = 150$, $w = 1$, $\gamma \approx 1.2 \times 10^{-3}$ and $v_f = 0.7$.

emission of photons by the qubit. Like in the case of the identical spins, we assume that if there are any bound states in the Fock space of the bosonic mode, then they are eigenstates of $\hat{\sigma}_z$

$$\begin{aligned} \tilde{\chi}_\uparrow(x) &= A_\uparrow(x) \begin{bmatrix} 1 \\ 0 \end{bmatrix} \\ \tilde{\chi}_\downarrow(x) &= A_\downarrow(x) \begin{bmatrix} 0 \\ 1 \end{bmatrix} \end{aligned} \quad (14)$$

and they have zero energy $\hat{H}_a \tilde{\chi}_{\uparrow(\downarrow)}(x) = 0$. In the x -representation of the mode operators, the energy equation becomes

$$\left[\left(v + \frac{w}{\sqrt{2}}x \right) \hat{\sigma}_x + i \frac{w}{\sqrt{2}} \frac{\partial}{\partial x} \hat{\sigma}_y \right] \tilde{\chi}_{\uparrow(\downarrow)}(x) = 0$$

which has solutions of the form

$$\begin{aligned} A_\uparrow(x) &= C_\uparrow e^{\frac{1}{2}(x + \frac{\sqrt{2}v}{w})^2} \\ A_\downarrow(x) &= C_\downarrow e^{-\frac{1}{2}(x + \frac{\sqrt{2}v}{w})^2}. \end{aligned} \quad (15)$$

Only the second solution is normalizable with $C_\downarrow = \pi^{-1/4}$ and is simply the x -representation of the coherent

state $|\alpha = -v/w\rangle = e^{-\frac{1}{2}|\frac{v}{w}|^2} \sum_{m_a} \frac{(-v/w)^{m_a}}{\sqrt{m_a!}} |m_a\rangle$ where $\hat{a}^\dagger \hat{a} |m_a\rangle = m_a |m_a\rangle$. This means there is only a single bound state and it exists in the spin- \downarrow subspace. The BC state protocol relies on there being two bound states, each one attached to different qubit states, that can be used to split the initial state into two distinguishable parts. Therefore, we conclude that the protocol will not work if the identical spins are replaced with a single bosonic mode.

The presence of a single bound state can be explained by the bulk-boundary correspondence, which asserts that a topological invariant, such as the winding number in 1D, counts the number of bound states at each boundary separating regions of different topology. In the case of N identical spins coupled to a qubit, there are two bound states because the Fock space has two boundaries at $\pm N/2$. However, for a single bosonic mode, the Fock space is only bounded from below by the vacuum, meaning there is only one edge and, thus, a single bound state. This bulk-boundary correspondence can be verified by calculating the mean-field winding number, where the mode operators are replaced with their coherent state expectation values $\langle \alpha | \hat{a} | \alpha \rangle = |\alpha| e^{-i\beta}$ leading to the expression

$$H_a = v\hat{\sigma}_x + w|\alpha|(\cos\beta\hat{\sigma}_x + \sin\beta\hat{\sigma}_y). \quad (16)$$

Comparing this equation with Eqns. (3) and (4), we see they are the same when the transformations $\sin\theta \rightarrow |\alpha|$ and $\phi \rightarrow \beta$ are made. Applying these transformations to the calculation of the winding number in Eq. (6) gives

$$W_a(\alpha) = \frac{1}{2} [1 + \text{sgn}(w|\alpha| - v)]. \quad (17)$$

Equation 17 shows that because α is unbounded from the above, there always exists a boundary between two topological regions at $|\alpha| = v/w$, however, because it is bounded from below, there is only a single boundary with one bound state accompanying it. In Figure 5 we plot the spin- \downarrow zero energy eigenstate of \hat{H}_a (red, solid) and compare it with the coherent state $|\alpha = -v/w\rangle$ (black, dashed). We truncate the number of excitations of the bosonic mode, N_a , to $N_a = 100$ and find excellent agreement between the two results.

D. Random noise in the driving

In general, the effect of the interactions between a system and an environment causes the destruction of quantum superpositions through a process called decoherence. Decoherence can come from many sources such as unwanted noise in laboratory equipment or from measurement processes. The stability of the bound states originates from the chiral symmetry which is maintained throughout the driving process, however, we can consider the case where the magnetic field driving the CS

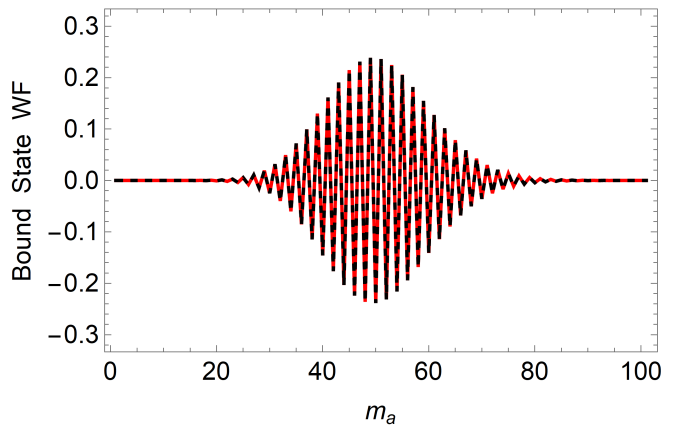


FIG. 5. Coherent bound states of a qubit coupled to a single bosonic mode. The zero energy bound state coupled to the spin- \downarrow state of the qubit (blue, solid) is compared with the coherent state $|-v/w\rangle$ (black, dashed) in Fock space labeled by m_a . The bound state at the right edge (red, solid) is an artifact of the truncation of the Hilbert space to $N_a = 100$ total Fock states. The parameter values are $w = 1$ and $v = 7$, so the coherent state is centered at $|\alpha|^2 = 49$.

is noisy. In general, all components of the magnetic field can introduce noise, however, the z -component is the most important because it breaks chiral symmetry in the Hamiltonian, so we consider the introduction of the small noisy term $\xi(t)\hat{\sigma}_z$. Assuming white noise such that $\langle \xi(t_1)\xi(t_2) \rangle \propto \delta(t_1 - t_2)$ and that the Born approximation can be applied, the density matrix evolves according to the master equation of the Lindblad form

$$\frac{d\rho(t)}{dt} = i [\rho(t), \hat{H}(t)] + \mathcal{D}[\hat{\sigma}_z]\rho(t) \quad (18)$$

where the first term describes the coherent evolution of the density matrix and

$$\mathcal{D}[\hat{A}]\rho = \frac{D}{2} (2\hat{A}\rho\hat{A} - \hat{A}^2\rho - \rho\hat{A}^2) \quad (19)$$

is the dissipator. The parameter D is proportional to the square of the z -component of the magnetic field which is assumed to be small. We note that a similar master equation describes weak continuous measurements of the $\hat{\sigma}_z$ eigenstates where the result of each measurement is not read out. In that case, the source of D is from the back-action of the measurement of $\hat{\sigma}_z$ on the system where the more accurate the measurement, the larger it is. Equation (18) describes a type of decoherence called dephasing which results in the scrambling of the phases of the wave function or in the case of the density matrix, decay of coherences which are contained in its off-diagonal elements.

In our protocol, the time needed to form a BC state is $t_{BC} = t_1 + t_2$ where $t_1 = (v_0 - w)/\gamma$ is the time it takes to reach the topological transition point at $v = w$ and t_2 is the time from t_1 when the wave function first splits into

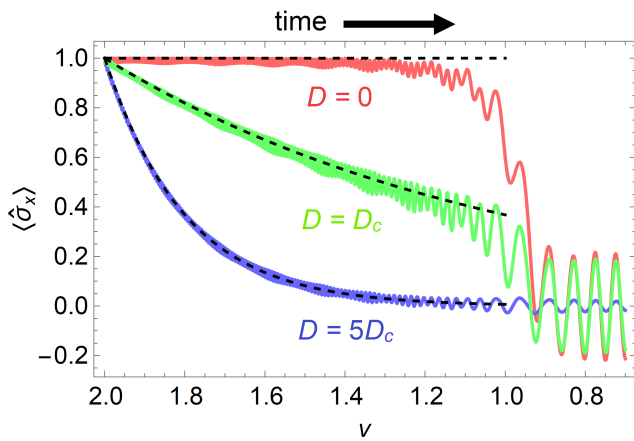


FIG. 6. Coherence of the CS as a function of v for different decoherence strengths as the system is driven through the topological phase transition point at $v = w$. The parameter values are $w = 1$ and $N = 100$.

a macroscopic superposition. We define the macroscopic superposition as forming when the separation between the peaks of the spin- \uparrow and spin- \downarrow components of the wave function become equal to one of their widths. Using the mean and standard deviation from the semiclassical bound state wave function in Eq. (9), the splitting occurs when $2n_b(t_2) = \sigma(t_2)$ where the time dependence comes from the driving of the spin-flip energy $v(t) = v_0 - \gamma t$. Solving for t_2 gives $t_2 \approx w / (128^{1/3} N^{2/3} \gamma)$. Due to the N dependence of t_2 , for sufficiently large N , t_1 becomes the dominant term resulting in $t_{BC} \approx (v_0 - w) / \gamma$.

In order for a BC state to form, the condition $t_{BC} \ll t_D$ must be satisfied, where t_D is the decoherence time. To simplify the analysis, we assume that throughout the driving process in the topologically trivial phase the initial state has high fidelity with the target bound state and that adiabaticity is maintained. This means that there is negligible coherent dynamics, so the first term in Eq. (18) can be ignored. Now the identical spins can be traced out, $\rho_{CS}(t) = \text{Tr}_S[\rho(t)]$, and we are left with a master equation in terms of the CS only

$$\frac{d\rho_{CS}(t)}{dt} \approx D [\hat{\sigma}_z \rho_{CS}(t) \hat{\sigma}_z - \rho_{CS}(t)]. \quad (20)$$

With the initial state being $|\psi(0)\rangle$ from Eq. (10), the master equation can be solved for each component of $\rho_{CS}(t)$ giving

$$\rho_{CS}(t) \approx \frac{1}{2} \begin{pmatrix} 1 & e^{-t/t_D} \\ e^{-t/t_D} & 1 \end{pmatrix} \quad (21)$$

where the decoherence time is $t_D = \frac{1}{2D}$. Therefore, there is a crossover region around $D_c = \frac{1}{2(v_0 - w)}$ where for $D \gg D_c$, the system will decohere before the BC state has a chance to form.

To confirm this analysis we plot the CS coherence, $\langle \hat{\sigma}_x(t) \rangle = \text{Tr}[\hat{\sigma}_x \rho(t)]$, as a function of v (time) for different values of D in Figure 6. In the absence of decoherence (red), $\langle \hat{\sigma}_x(t) \rangle$ remains close to unity, while significant decoherence (blue) results in exponential decay in the topologically trivial region ($v > 1$). Each of the three curves closely follows the predicted result of $\langle \hat{\sigma}_x(t) \rangle = e^{-t/t_D}$ (dashed, black curves) from Eq. (21). The minor oscillations observed in the trivial region stem from the initial state in Eq. (10) having imperfect overlap with the target eigenstate in Eq. (A4). Due to not being completely adiabatic, the amplitude of the small oscillations become amplified in the topologically nontrivial region ($v < 1$), however, they still oscillate around the predicted value of zero. The abrupt drop in the nontrivial region signifies the formation of the BC state, explicitly observed by utilizing the expressions for the bound states in Eq. (9) to calculate the expectation value, resulting in $\langle \hat{\sigma}_x(t) \rangle_B = e^{-\frac{n_b(t)^2}{2\sigma(t)^2}}$. As the driving shifts the states to larger n_b , the coherence of the CS exponentially decays.

IV. CONCLUSIONS AND DISCUSSION

We have demonstrated that in a CS model obeying chiral symmetry, a topological phase transition takes place. In the topologically nontrivial phase, a pair of protected bound states emerges within the Fock space of the identical spins surrounding the CS. Each member of this pair is coupled to a different state of the CS. Notably, these bound states exhibit a unique characteristic — their positions can be adjusted by tuning parameters in the system, distinguishing them from typical bound states found in many condensed matter systems. This distinction stems from the spherical geometry of the Hilbert space of identical spins, which differs from the circular and toroidal geometry found in the quasi-momentum of 1D and 2D periodic lattices, respectively.

The mobility of the bound states is pivotal in the protocol employed for generating BC states. Our approach involves having a large overlap between an initial spin coherent state and a target eigenstate of the Hamiltonian which will become the protected bound states, then adiabatically driving the system to induce the splitting of the bound states into a macroscopic superposition within Fock space. We achieve the large overlap by initializing the system in the topologically trivial phase where the bound states have the same form as the spin coherent state. To ensure an equal overlap with the two bound states, we initialize the CS in an equal superposition of its two states. The splitting is achieved by adiabatically driving the system through the transition point into the topologically nontrivial phase where the bound states become mobile. The driving results in the CS spin-up part of the state moving in one direction in Fock space while the spin-down part moves in the other direction. When the system is driven deep enough into the nontriv-

ial phase, the two parts of the state have exponentially small overlap and a BC state is formed.

Although the version of the CS model we analyzed is quite simple, it can be expanded to be more general because the main criterion needed to generate a BC state is the presence of mobile topologically protected bound states. This requirement means that the Hamiltonian must obey chiral symmetry which leaves room for additional terms of the form $\hat{\sigma}_x f(\hat{S}_x, \hat{S}_y, \hat{S}_z)$ and $\hat{\sigma}_y g(\hat{S}_x, \hat{S}_y, \hat{S}_z)$ where f and g denote general functions of the identical spins' operators. The zero energy eigenstates (there may be many pairs of such states depending on the functions) will also be eigenstates of the chiral symmetry operator, $\hat{\sigma}_z$, and will serve as the target BC state(s) in similar driving protocols to the one considered in this paper. In experiments, it may be impossible to neglect chiral symmetry-breaking terms. Two such terms that may appear in the CS model are $v_z \hat{\sigma}_z$ and $w_z \hat{\sigma}_z \hat{S}_z$. Separately they destroy the bound states, however, together it may be possible to tune the parameters of the system such that their contributions cancel for a given bound state, $v_z \hat{\sigma}_z + w_z \hat{\sigma}_z \langle \hat{S}_z \rangle_B = 0$. Although further analysis is necessary to explore this possibility, it could potentially offer a workaround of certain persistent symmetry-breaking terms.

ACKNOWLEDGMENTS

D.H.J.O. acknowledges the support of the Natural Sciences and Engineering Research Council of Canada through Discovery Grant No. RGPIN-2017-06605.

Appendix A: Target eigenstate wave functions in the topologically trivial phase

We start by deriving an expression for the identical spins' component of the bound state in the topologically trivial phase by diagonalizing Eq. (3) giving

$$E_{\pm} = \pm \sqrt{v^2 + w^2 \left(1 - \frac{4n^2}{N^2}\right) + 2vw \cos \phi \sqrt{1 - \frac{4n^2}{N^2}}} \quad (\text{A1})$$

where we have used the relation $n = \frac{N}{2} \cos \theta$. The overall sign signifies whether the CS is in an even (+) or odd (−) superposition and corresponds to the top and bottom energy bands, respectively, in Figure 4 (a). In the trivial phase, the even parity bound state is the ground state of the top band which we know is centered at $(n, \phi) = (0, \pi)$, so we expand the energy around those points keeping up to quadratic order in both variables

$$E_+ \approx \frac{vw}{2(v-w)} (\phi - \pi)^2 + \frac{2w}{N^2} n^2. \quad (\text{A2})$$

In the semiclassical theory, n and ϕ are conjugate variables obeying the commutation relation $[n, \phi] = -i$, so we can make the transformation $\phi \rightarrow i \frac{d}{dn}$ resulting in

$$E_+ \approx \frac{vw}{2(v-w)} \left(i \frac{d}{dn} - \pi\right)^2 + \frac{2w}{N^2} n^2 \quad (\text{A3})$$

where the energy describes an harmonic oscillator (with momentum shifted by π) whose mass and frequency are $\frac{(v-w)}{vw}$ and $\frac{2w}{N} \sqrt{\frac{v}{v-w}}$, respectively. The ground state of the system is

$$B_0(n) \approx \left(\frac{2}{\pi N} \sqrt{1 - \frac{w}{v}}\right)^{1/4} e^{i\pi n} e^{-\sqrt{1 - \frac{w}{v}} \frac{n^2}{N}} \quad (\text{A4})$$

where the phase factor $e^{i\pi n}$ comes from the π shift of ϕ . One can see that for as $w/v \rightarrow 0$, $B_0(n)$ approaches the spin coherent state in Eq. (11). Therefore, for larger v_0 the spin coherent state has a larger initial overlap with Eq. (A4) and if the system is evolved adiabatically, the final overlap will also be larger as shown in Figure 4 (b).

-
- [1] E. Schrödinger, Die gegenwärtige Situation in der Quantenmechanik, *Naturwissenschaften* **23**, 807 (1935).
- [2] C. Monroe, D. M. Meekhof, B. E. King, and D. J. Wineland, A “Schrödinger Cat” Superposition State of an Atom, *Science* **272**, 1131 (1996).
- [3] A. Ourjoumteev, H. Jeong, R. Tualle-Brouiri, and P. Grangier, Generation of optical “Schrödinger cats” from photon number states. *Nature* **448**, 784 (2007).
- [4] S. Deléglise, I. Dotsenko, C. Sayrin, J. Bernu, M. Bruen, J.-M. Raimond, and S. Haroche, Reconstruction of non-classical cavity field states with snapshots of their decoherence, *Nature* **455**, 510 (2008).
- [5] B. Vlastakis, G. Kirchmair, Z. Leghtas, S. E. Nigg, L. Frunzio, S. M. Girvin, M. Mirrahimi, M. H. Devoret, and R. J. Schoelkopf, Deterministically Encoding Quantum Information Using 100-Photon Schrödinger Cat States, *Science* **342**, 607 (2013).
- [6] D. Leibfried, E. Knill, S. Seidelin, J. Britton, R. B. Blakestad, J. Chiaverini, D. B. Hume, W. M. Itano, J. D. Jost, C. Langer, R. Ozeri, R. Reichle, and D. J. Wineland, Creation of a six-atom “Schrödinger cat” state, *Nature* **438**, 639 (2005).
- [7] J. Mumford, Two-particle topological Thouless spin pump, *Phys. Rev. A* **107**, 033302 (2023).
- [8] D. J. Wineland, Nobel Lecture: Superposition, entanglement, and Schrödinger’s cat, *Rev. Mod. Phys.* **85**, 1103 (2013).
- [9] H.-Y. Lo, D. Kienzler, L. de Clercq, M. Marinelli, V. Negnevitsky, B. C. Keitch, and J. P. Home, Spin-motion entanglement and state diagnosis with squeezed oscillator

- wavepackets, *Nature* **521**, 336 (2015).
- [10] D. Kienzler, C. Flühmann, V. Negnevitsky, H.-Y. Lo, M. Marinelli, D. Nadlinger, and J. P. Home, Observation of Quantum Interference between Separated Mechanical Oscillator Wave Packets, *Phys. Rev. Lett.* **116**, 140402 (2016).
- [11] W.-B. Gao, C.-Y. Lu, X.-C. Yao, P. Xu, O. Gühne, A. Goebel, Y.-A. Chen, C.-Z. Peng, Z.-B. Chen, and J.-W. Pan, Experimental demonstration of a hyper-entangled ten-qubit Schrödinger cat state, *Nat. Phys.* **6**, 331 (2010).
- [12] S. Haroche and J.-M. Raimond, *Exploring the Quantum: Atoms, Cavities, and Photons*, Oxford Univ. Press (2006).
- [13] M. Bold, M. Fadel, Y. Yang, U. von Lüpke, P. Martin, A. Bruno, and Y. Chu, Schrödinger cat states of a 16-microgram mechanical oscillator, *Science* **380**, 274 (2023).
- [14] B. Hacker, S. Welte, S. Daiss, A. Shauket, S. Ritter, L. Li, and G. Rempe, Deterministic creation of entangled atom-light Schrödinger-cat states, *Nat. Photonics* **13**, 110 (2019).
- [15] B. Vlastakis, A. Petrenko, N. Ofek, L. Sun, Z. Leghtas, K. Silwa, Y. Liu, M. Hatridge, J. Blumoff, L. Frunzio, M. Mirrahimi, L. Jiang, M. H. Devoret, and R. J. Schoelkopf, Characterizing entanglement of an artificial atom and cavity state with Bell's inequality, *Nat. Commun.* **6**, 8970 (2015).
- [16] S. L. Braunstein, and P. van Loock, Quantum information with continuous variables, *Rev. Mod. Phys.* **77**, 513 (2005).
- [17] A. Hutton and S. Bose, Mediated entanglement and correlations in a star network of interacting spins, *Phys. Rev. A* **69**, 042312 (2004).
- [18] H. P. Breuer, D. Burgarth, and F. Petruccione, *Phys. Rev. B* **70**, 045323 (2004).
- [19] K. A. Al-Hassanieh, V. V. Dobrovitski, E. Dagotto, and B. N. Harmon, *Phys. Rev. Lett.* **97**, 037204 (2006).
- [20] S. S. Garmon, P. Ribeiro, and R. Mosseri, *Phys. Rev. E* **83**, 041128 (2011).
- [21] M. R. Dennis and M. A. Alonso, Swings and roundabouts: optical Poincaré spheres for polarization and Gaussian beams, *Phil. Trans. R. Soc. A* **375**, 20150441 (2017).
- [22] R. Gutiérrez-Cuevas, S. A. Wadood, A. N. Vamivakas, and M. A. Alonso, Modal Majorana Sphere and Hidden Symmetries of Structured-Gaussian Beams, *Phys. Rev. Lett.* **125**, 123903 (2020).
- [23] T. Zibold, E. Nicklas, C. Gross, and M. K. Oberthaler, Classical Bifurcation at the Transition from Rabi to Josephson Dynamics, *Phys. Rev. Lett.* **105**, 204101 (2010).
- [24] M. Albiez, R. Gati, J. Fölling, S. Hunsmann, M. Cristiani, and M. K. Oberthaler, Direct Observation of Tunneling and Nonlinear Self-Trapping in a Single Bosonic Josephson Junction, *Phys. Rev. Lett.* **95**, 010402 (2005).
- [25] S. Levy, E. Lahoud, L. Shomroni, and J. Steinhauer, The a.c. and d.c. Josephson effects in a Bose-Einstein condensate, *Nature* **449**, 579 (2007).
- [26] I. Bausmerth, U. R. Fischer, and A. Posazhennikova, Quantum top inside a Bose-Einstein-condensate Josephson junction, *Phys. Rev. A* **75**, 053605 (2007); U. R. Fischer, Christian Iniotakis, and Anna Posazhennikova, Coherent single atom shuttle between two Bose-Einstein condensates, *Phys. Rev. A* **77**, 031602(R) (2008).
- [27] M. Rinck and C. Bruder, Effects of a single fermion in a Bose Josephson junction, *Phys. Rev. A* **83**, 023608 (2011).
- [28] F. Mulansky, J. Mumford, and D. H. J. O'Dell, Impurity in a Bose-Einstein condensate in a double well, *Phys. Rev. A* **84**, 063602 (2011).
- [29] J. Mumford, J. Larson, and D. H. J. O'Dell, Impurity in a bosonic Josephson junction: Swallowtail loops, chaos, self-trapping, and Dicke model, *Phys. Rev. A* **89**, 023620 (2014).
- [30] J. Mumford and D. H. J. O'Dell, Critical exponents for an impurity in a bosonic Josephson junction: Position measurement as a phase transition, *Phys. Rev. A* **90**, 063617 (2014).
- [31] J. Chen, K. Keiler, G. Xianlong, and P. Schmelcher, Impurity-induced quantum chaos for an ultracold bosonic ensemble in a double well, *Phys. Rev. A* **104**, 033315 (2021).
- [32] R. Gerritsma, A. Negretti, H. Doerk, Z. Idziaszek, T. Calarco, and F. Schmidt-Kaler, Bosonic Josephson Junction Controlled by a Single Trapped Ion, *Phys. Rev. Lett.* **109**, 080402 (2012).
- [33] J. Joger, A. Negretti, and R. Gerritsma, Quantum dynamics of an atomic double-well system interacting with a trapped ion, *Phys. Rev. A* **89**, 063621 (2014).
- [34] M. R. Ebgha, S. Saeidian, P. Schmelcher, and A. Negretti, Compound atom-ion Josephson junction: Effects of finite temperature and ion motion, *Phys. Rev. A* **100**, 033616 (2019).
- [35] F. Schmidt, D. Mayer, Q. Bouton, D. Adam, T. Lausch, N. Spethmann, and A. Widera, Quantum Spin Dynamics of Individual Neutral Impurities Coupled to a Bose-Einstein Condensate, *Phys. Rev. Lett.* **121**, 130403 (2018).
- [36] Q. Bouton, J. Nettersheim, D. Adam, F. Schmidt, D. Mayer, T. Lausch, e. Tiemann, and A. Widera, Single-Atom Quantum Probes for Ultracold Gases Boosted by Nonequilibrium Spin Dynamics, *Phys. Rev. X* **10**, 011018 (2020).
- [37] D. Adam, Q. Bouton, J. Nettersheim, S. Burgardt, and A. Widera, Coherent and dephasing spectroscopy for single-impurity probing of an ultracold bath, *Phys. Rev. Lett.* **129**, 120404 (2022).
- [38] R. Gutiérrez-Cuevas, D. H. J. O'Dell, M. R. Dennis, and M. A. Alonso, Exactly solvable model behind Bose-Hubbard dimers, Ince-Gauss beams, and aberrated optical cavities, *Phys. Rev. A* **107**, L031502 (2023).